Optimized LCC-Series Compensated Resonant Network for Stationary Wireless EV Chargers

Ali Ramezani, *Student Member, IEEE,* Shahrokh Farhangi*, Member, IEEE, Hossein Iman-Eini, Senior Member, IEEE,* Babak Farhangi*, Senior Member, IEEE,* Ramin Rahimi*,* Gholam Reza Moradi

Abstract— In this paper, an optimal design procedure for LCC-series compensation network is proposed for a stationary wireless Electric Vehicle (EV) charger. The main focus of this paper is to optimize the resonant network suitable for a wide range of operation from no-load to full power operation. The conventional methods only consider the full load condition to design the resonant network; in contrast, the proposed method employs a Time-Weighted Average Efficiency (TWAE) for different coupling conditions to achieve high efficiency over a wide load range including light-load and no-load operation. The resonant network is tuned to realize Zero Voltage Switching (ZVS) for the primary side inverter. Moreover, a Finite Element Analysis (FEA) is performed to calculate self and mutual inductances as well as core losses for magnetic couplers. In order to validate the feasibility of the proposed design, a 1 kW/85 kHz prototype with circular magnetic couplers is implemented. According to simulations and experiments, flat profiles for both efficiency and output voltage against output power variations are achieved. Experimental results demonstrate a 94.8% peak efficiency for the full-load operating.

***Index Terms*— Optimization, resonant converter, stationary charging, Wireless Power Transfer (WPT), Zero Voltage Switching (ZVS).**

I. INTRODUCTION

Wireless Power Transfer (WPT) is an attractive solution for charging the Electric Vehicles (EV). One of the attractive features of the WPT is that it can be used for dynamic charging of EVs [1]–[3]. High power WPT charging systems can evolve transportation systems. For instance, in public transport, the electric buses can be charged in the bus stations or on the roadway [4]. In, [5], [6] a 50 kW inductive WPT system for the public transportation application is designed based on the efficiency-power density with Pareto optimization method. Additionally, this technology is used in railway public transportation systems in which the train can be energized through the railway [7]. In [8], a hybrid bidirectional WPT system is proposed, which is capable of providing constant power over a wide range of vertical and horizontal misalignment.

Several geometries for the magnetic coupler have been discussed in [9, 10]. The circular geometry offers higher magnetic coupling coefficient (k) for a specific area [11], which leads to a more efficient energy conversion as well as higher power density for EV charging system. In addition, in [12] it is discussed that the circular magnetic coupler has better performance and power density in comparison with the segmented and rectangular structures. In [13]–[17], the WPT charging system utilizes circular pads as coupling structures for EV applications. Circular structures can be modified towards higher coupling performance [17, 18]. In addition, passive repeaters extend the transmition distance [20]–[22]. In [23], a closed form solution for the mutual inductance of two ferrite-less circular coils is presented , in which both vertical and horizontal missaligment conditions are addressed.

Series and LCC configurations are among the popular compensation networks for the resonant converters that have been compared in recent studies [24]–[26]. The series compensated resonant network operates as a voltage source at the resonant frequency. It suffers from the short circuit occurrence on the load side [27]. In a WPT system, the absence of the secondary side (the receiver coil) causes the series compensated network of the primary side to be short circuit. In the open-loop operation, in this configuration by increasing the coupling coefficient, the output power decreases [14].

LCC compensation network has been utilized for the primary side of WPT systems [28]–[31]. A well-designed LCC compensated network operates as a constant current converter [32]. LCC compensation network provides a constant current for the primary side coil. Thus, a constant voltage is induced on the secondary coil, independent of the load variations. If the induced voltage on the secondary coil remains constant, the output voltage remains independent of the load variations. By using a series resonant compensation on the secondary side, the constant induced voltage on the secondary side can be delivered to the load with a constant voltage characteristics [27]. Therefore, LCC-Series compensation network provides a voltage source feature for the WPT system.

Compared to the series resonant converter, LCC network includes more components. In contrast, the capacitors voltage stress is less in LCC topology [14]. In [33], an integrated LCC

Manuscript received July 31, 2017; revised November 19, 2017 and February 17, 2018; accepted May 9, 2018.

A. Ramezani is with the Department of Electrical and Computer Engineering, McMaster University, Hamilton, ON, Canada (e-mail: ramezana@mcmaster.ca).

S. Farhangi, H. Iman-Eini, R. Rahimi, and G. R. Moradi are with the School of Electrical and Computer Engineering, University of Tehran, Tehran, Iran (e-mail: farhangi@ut.ac.ir; imaneini@ut.ac.ir; raminrahimi@ut.ac.ir; gh.r.moradi@ut.ac.ir).

B. Farhangi is with GAF, Parsippany, NJ 07054, USA (e-mail: farhangi@ieee.org).

compensation topology is presented to reduce the size and weight of the resonant network. Furthermore, LCC compensated network is efficient at light loads [14]. In this paper, LCC topology is chosen for the primary side and series compensation network for the secondary side of the proposed stationary wireless charging system.

Various methods have been discussed to propose an optimal design for resonant networks. As an example, in [34], a highly efficient dynamic charging WPT system is discussed; the output voltage ripple remains low despite magnetic coupling variations. In contrast, in a stationary charging application, the coupling does not vary over the charging time. However, the output power varies from no-load to nominal rated power. A semi-flat efficiency profile over the wide range of output power is preferred for stationary WPT chargers. The output voltage needs to remain within upper and lower boundaries for various operating points.

The main focus of this paper is to design an optimized LCC-series resonant network for the stationary wireless charging system. Mathematical models of the LCC compensated network for the primary side and the series compensating network for the secondary side are developed. In addition, the overall system model is optimized which involves switching and conductive loss of the H-Bridge inverter, core and conductive loss of magnetic components, dielectric loss of the resonant capacitors, and secondary side rectifiers. Also, the proposed design method is based on the Time Weighted Average Efficiency (TWAE) index, which leads to an optimal solution for different operating conditions [35]. This proposed optimized design method results in finding optimal values for the components of the resonant network.

In order to realize Zero Voltage Switching (ZVS), a constraint is employed in the optimization problem. The proposed design method is compared with conventional methods. According to numerical calculations, simulations and experimental results, the proposed method results in a design with improved efficiency and output voltage regulation compared to the conventional methods.

Owing to the proposed design procedure method, both the efficiency and voltage gain benefit from a flat curve across the entire operating range. The output voltage remains almost constant and independent of the load conditions. In [24] a double-sided LCC converter is used to achieve a flat efficiency curve. However, in this paper by using LCC-Series and its proposed tuning method, not only the number of components reduced but also a flat efficiency profiles are achieved.

The paper is structured as follows; in Section II, a theoretical analysis is presented for the LCC-series compensated resonant network. Additionally, the magnetic couplers and the calculating method for mutual and self-inductances, and core losses are presented. In Section III, an optimization problem is defined to apply the stationary charging application practical constraints. The optimized result is compared with the results from earlier methods. Experimental and simulation results are presented in Section IV. Finally, the conclusions are summarized in Section V.

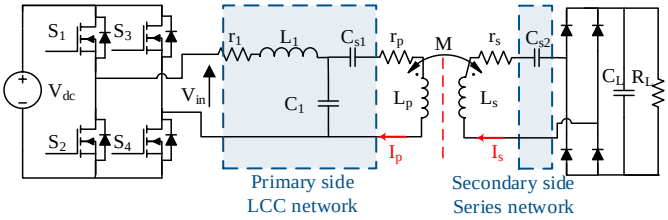

Fig. 1. Proposed topology with an LCC-Series compensation network

II. Proposed Topology And Analysis

A. Steady-State System Equations

The LCC-series compensated topology is shown in Fig. 1. WPT's steady-state is analyzed through fundamental harmonic approximation (FHA) [36]. In this section, for simplicity of the analysis, magnetic core losses of the inductors and resonant tank are neglected. This approximation is acceptable because of the low flux density of the ferrite bars. Considering only the copper losses of the magnetic couplers, the equivalent circuit of the proposed WPT system is presented in Fig. 2. The Fourier series of the inverter output voltage V_{in} and the RMS value of the fundamental component V_{in}^{rms} are as follows:

$$V_{in} = \sum_{n=1}^{\infty} \frac{4V_{dc}}{n\pi} \sin(\frac{\theta}{2}) \sin(n\omega t) \tag{1}$$

$$V_{in}^{rms} = \frac{2\sqrt{2}V_{dc}}{\pi} \sin(\frac{\theta}{2}) \tag{2}$$

In (1), θ is the switching phase shift between the legs of the H-bridge inverter and ω is the operating angular frequency. Assuming a large value for C_L, the equivalent resistance of the rectifier in the secondary side R_{eq}, can be written as:

$$R_{eq} = \frac{8}{\pi^2} R_L \tag{3}$$

According to Fig. 2, the secondary Z_s, primary Z_p, and input Z_{in} impedance are extracted as:

$$Z_s = R_{eq} + r_s + j\omega\left((L_s - M) - \frac{1}{\omega^2 C_{s2}}\right) \tag{4}$$

$$Z_{ps} = j\omega M \parallel Z_s = j\omega M + \frac{(M\omega)^2}{R_{eq} + r_s + j\omega(L_s - \frac{1}{C_{s2}\omega^2})} \tag{5}$$

$$Z_p = r_p + j\omega\left((L_p - M) - \frac{1}{\omega^2 C_{s1}}\right) + Z_{ps} \tag{6}$$

$$Z_{in} = r_1 + \omega L_1 j + Z_p \parallel \frac{1}{\omega C_1} \tag{7}$$

The input phase angle ϕ, between V_{in} and I_{in} is calculated by decomposing the real and imaginary parts of the input impedance as follows:

$$I_{in} = \frac{V_{in}}{Z_{in}} = \left|\frac{V_{in}}{Z_{in}}\right| \angle\phi \tag{8}$$

$$\phi = \angle Z_{in} = \tan^{-1} \frac{\Im\{Z_{in}\}}{\Re\{Z_{in}\}} \tag{9}$$

This article has been accepted for publication in a future issue of this journal, but has not been fully edited. Content may change prior to final publication. Citation information: DOI 10.1109/TIE.2018.2840502, IEEE Transactions on Industrial Electronics

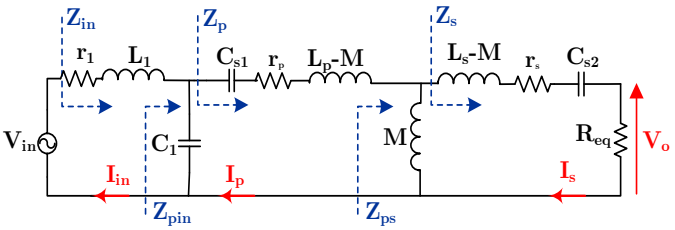

Fig. 2. The equivalent circuit for the proposed WPT system (one-to-one turns ratio)

$$\Re\{Z_{in}\} = r_1 + \Re\{Z_{pin}\} = r_1 + \Re\{Z_p\}\frac{\left[\left(1-C_1\omega\Im\{Z_p\}\right)+C_1\omega\Im\{Z_p\}\right]}{\left(1-C_1\omega\Im\{Z_p\}\right)^2+\left(C_1\omega\Re\{Z_p\}\right)^2} \quad (10)$$

$$\Re\{Z_p\} = r_p + \frac{(\omega M)^2\,\Re\{Z_s\}}{\left(\Re\{Z_s\}+\omega M\right)^2+\Re\{Z_s\}^2} \quad (11)$$

$$\Re\{Z_s\} = r_s + R_{eq} \quad (12)$$

$$\Im\{Z_{in}\} = \omega L_1 + \Im\{Z_{pin}\} = \omega L_1 - \frac{\omega C_1\Im\{Z_p\}\Re\{Z_p\}}{\left(1-C_1\omega\Im\{Z_p\}\right)^2+\left(C_1\omega\Re\{Z_p\}\right)^2} \quad (13)$$

$$\Im\{Z_p\} = \omega\left(L_1-\frac{1}{C_{s1}\omega^2}\right)+\Im\{Z_{ps}\} = \omega\left(L_1-\frac{1}{C_{s1}\omega^2}\right)-\frac{(M\omega)^2\left(\Im\{Z_s\}+M\omega\right)}{\Re\{Z_s\}^2+\left(\Im\{Z_s\}+M\omega\right)^2} \quad (14)$$

$$\Im\{Z_s\} = \omega\left(L_s - M - \frac{1}{\omega^2 C_{s2}}\right) \quad (15)$$

M is the mutual inductance of the transformer, L_p and L_s are the primary and secondary self-inductances, respectively. The input P_{in}, and output power P_{out} of the WPT system is expressed:

$$P_{in} = |I_{in}|^2\,\Re\{Z_{in}\} \quad (16)$$

$$P_{out} = |I_s|^2 R_{eq} \quad (17)$$

The output voltage (V_o) is dependent on the mutual coupling, frequency, and the inverter output voltage (V_{in}). As it was discussed before, in a stationary charging application, the mutual inductance is constant during the charging process. Therefore, in a fixed operating frequency, the output voltage can be controlled by controlling the primary side switching phase angle (θ) [37]–[39].

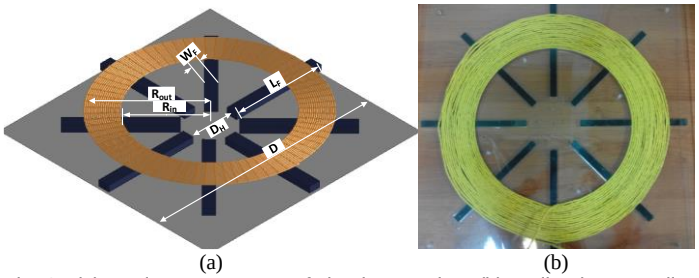

(a) (b)

Fig. 3. (a) Design parameters of circular couplers (b) realized WPT coil

TABLE I
DESIGN SPECIFICATIONS

Parameter	Value
R_{in}	180 mm
R_{out}	261 mm
W_f	28 mm
L_f	240 mm
D_H *(Hole diameter of the ferrite strips)*	60 mm
D	600 mm
Number of turns	18
Number of ferrite strips	8
Thickness of ferrite strips	16 mm
Volume of ferrite	860.1 cm^3

B. Magnetic Couplers

Magnetic couplers are the key elements of a wireless power transfer system. Design parameters of the circular magnetic couplers are illustrated in Fig. 3 (a). In this paper, a circular pad with a 600 mm diameter is considered for both primary and secondary coils. The design of the magnetic couplers is out of the scope of this paper; however, the design procedure is based on the guidelines presented in [40]. Design parameters of the magnetic couplers are listed in Table I. The self and mutual inductances and core losses are calculated to be used in the optimization of the circuit which will be discussed in the next section. In Fig. 3 (b), the realized magnetic couplers for the experimental setup is shown. In the experimental setup, Litz wire is used for making the coils to reduce the skin effect that results in reducing the ac resistance. This helps to have a higher quality factor for the coils and increase the system efficiency. The loosely coupled transformer is built with 18 turns on both primary and secondary side which consists of a Litz wire with a strand diameter of 0.2 mm.

The distribution of the magnetic flux in the materials is calculated using finite element method (FEM), which is

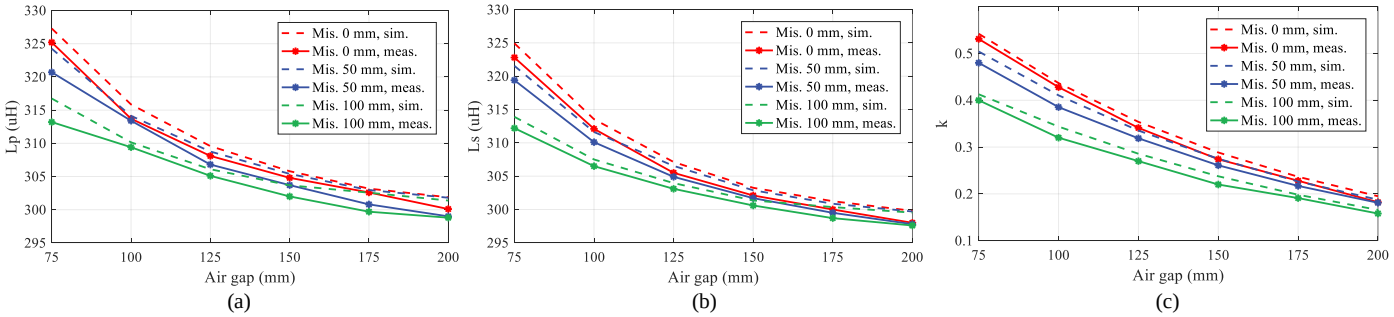

(a) (b) (c)

Fig. 4. Measurement and simulation results: (a) Primary self inductance (b) secondary self inductance (c) coupling coefficient

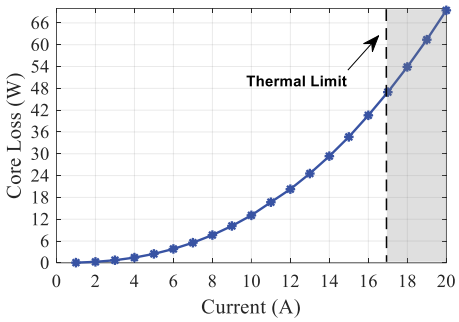

Fig. 5. Magnetic core loss of circular pads as a function of current

performed in a 3D-FEM software, ANSYS Maxwell. Fig. 4(a) and Fig. 4 (b) depict the simulation and experimental measurement results for variations of the primary, and secondary inductances under different lateral misalignment conditions at different air gaps. The small average error at all measured positions between the simulation results and the measurements illustrates an excellent accordance of the FEM simulations. The variations of *k*, is presented in Fig. 4 (c) as a function of the air gap in different lateral alignment positions.

According to SAE J2954 standard, the nominal operating frequency for light-duty vehicles is set to 85 kHz. In Fig. 5, total core loss variations are calculated as a function of the winding current at this frequency, for different current excitations. Increasing the circulating reactive current in coils and resonant tank leads to increasing copper and core losses in the magnetic pads. In summary, an optimal design is a trade-off between the energy storage components' losses and other goals such as open circuit induced voltage on the secondary coil or maximum transferable power. The results of this section, which includes the variations of mutual and self-inductances and core losses, are used in the optimization of the resonant converter, which is presented in the next section.

III. Optimization

In order to design a high-efficiency WPT system, the objective function, constraints, predefined parameters and system equations have to be defined. These are presented in the following subsections.

A. Objective Function

In earlier works, a high-efficiency resonant converter is designed for a specific operating point. In contrast, in this paper, the goal is to achieve a high-performance design for a wide range of load variations. Output power varies in the battery charger application. A time-weighted average efficiency index has to be used to satisfy this need. This objective function for a Li-ion battery is defined as [35]:

$$TWAE = 0.033\eta_B + 0.767\eta_D + 0.126\eta_A + 0.074\eta_C \quad (18)$$

In (18), η_A, η_B, η_C, and η_D are the system efficiencies in each operating points of A to D, which are presented in Fig. 6. However, in the WPT application, the objective function has to be defined as a function of the coupling coefficient of the magnetic couplers. This coefficient varies due to misalignment between the transmitter and receiver coils that result in the variation of the output power. The modified objective function for this application is defined as follows:

$$Max\left(\sum_{k_i \in K_n}\sum_{P_i \in P_n} W_{Pi} \times \eta_{P_i,k_i}\right) \quad (19)$$

Each η_{P_i,k_i} is the efficiency of the operating point with the output power of P_i and coupling factor of k_i. For instance, the objective function at k_1 is defined as follows:

$$Max\left(0.033\eta_{B,k_1} + 0.767\eta_{D,k_1} + 0.126\eta_{A,k_1} + 0.074\eta_{C,k_1}\right) \quad (20)$$

Based on (19), the objective function is defined to take all operating points into account except the absence of the secondary side ($k \simeq 0$). In no-load condition, there is no output power and the efficiency will be zero. By defining a set of normal operating points $P_n = \{P_B, P_D, P_A, P_C\}$ and K_n, the weighted efficiency is calculated for the candidate operating points. In this definition, W_{Pi} is the weighted value for each operating point. Using the proposed objective function in (19), results in a system with a more flat efficiency curve compared to the conventional designs.

B. Efficiency and Power Loss Calculation

Minimizing the losses is an important aspect of the WPT system design. The losses of the inverter diodes and MOSFETs are dependent on the input current of the resonant network I_{in}, and the phase angle of Z_{in}. The LCC compensation network is considered to have an inductive imaginary part to achieve ZVS for inverter switches. The turn-on losses of the MOSFETs is neglected. Conduction and switching losses of the MOSFETs are defined in (21). The anti-parallel diodes are modeled as an equivalent series resistance R_{diode} and on-state voltage U_{d0}.

$$P_{loss\_in} = 4P_{loss\_mosfet} + 4P_{loss\_diode} \quad (21)$$

$$P_{loss\_mosfet} = R_{ds(on)} I^2_{mosfet\_rms} + 2V_{dc} I_{mosfet} f\left(t_r + t_f\right) \quad (22)$$

$$P_{loss\_diode} \simeq U_{d0} I_{diode\_ave} + R_{diode} I^2_{diode\_rms} \quad (23)$$

By having a lag resonant network from the inverter side, the input current has a specific phase angle in terms of the inverter output voltage. The input impedance phase angle is dependent on the operating frequency, *k* and output resistive load. Below, anti-parallel diode and MOSFET currents I_{mosfet_rms} are calculated as a function of the input phase angle and amplitude of input current:

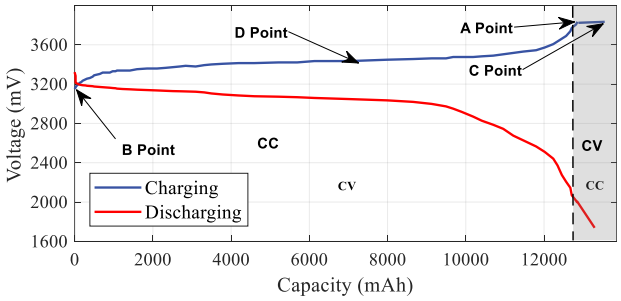

Fig. 6. Typical charging profile of Li-on battery redrawn from [34]

$$I_{mosfet\_rms} = |I_{in}|\sqrt{\frac{2(\pi-\phi)+\sin(2\phi)}{8\pi}} \quad (24)$$

$$I_{diode\_rms} = |I_{in}|\sqrt{\frac{2\phi-\sin(2\phi)}{8\pi}} \quad (25)$$

$$I_{diode\_ave} = \sqrt{2}|I_{in}|\frac{\cos\phi-1}{\omega} \quad (26)$$

In the next step, the inductor losses are included in the model. The conductive losses are dominant in L_1, as calculated below:

$$P_{c\_L1} = r_1 I_{in}^2 + P_{core\_L1} \quad (27)$$

$$P_{core\_L1} = k_i f^{\alpha} B^{\beta} V \quad (28)$$

In (26), r_1 is the ac resistance of the windings. It is calculated employing the modified Dowell's method for Litz-wire windings [41], [42]. In (27), k_i, α, and β are determined by the datasheet of the core material. Similarly, the core loss and conductive losses of the magnetic couplers is given in (28):

$$P_{loss\_p} = r_p I_p^2 + P_{core\_p} \quad (29)$$

$$P_{loss\_s} = r_s I_s^2 + P_{core\_s} \quad (30)$$

Where, r_p and r_s are the primary and secondary winding resistance. In order to have an accurate model for system losses, in (28) and (29), core losses of the magnetic couplers, P_{core_p} and P_{core_s} are modeled as a function of excitation currents. The nonlinear behavior and saturation of the core material are included in this FEM core loss analysis. Noticeably for this application, the capacitors need to have low changes in the capacitance value ($\Delta C/C < 2\%$) and low equivalent series resistance and parasitic inductance. Considering the dielectric characteristic of capacitors, the losses of resonant capacitors in primary and secondary is given in (30):

$$P_{loss\_cap} = \frac{\tan\delta(f)}{2\pi f}\left(\frac{I_{in}^2}{C_1}+\frac{I_p^2}{C_{s1}}+\frac{I_s^2}{C_{s2}}\right) \quad (31)$$

Finally, assuming that the output voltage of the diode bridge is constant, the power loss of the secondary side bridge rectifier is calculated as:

$$P_{loss\_bridge} = 4\left(U_{d0\_bridge}\frac{I_o}{2}+R_{d\_bridge}\left(\frac{I_o}{\sqrt{2}}\right)^2\right) \quad (32)$$

$$I_o = \sqrt{\frac{P_{out}}{R_{eq}}} \quad (33)$$

C. Constraints and Fixed Parameters

Several constraints are governed for a practical design by standards as well as application requirements. The WPT couplers core losses are extracted from FEA software, and in this optimization method, the authors consider it as a function of the excitation current, which has been presented in the previous section. In addition, the primary and secondary side inductances are defined as a function of the coupling coefficient based on the measurements which presented in section II.

It is assumed that the input dc voltage is constant and the output capacitor is big enough to maintain a constant voltage in each switching cycle.

In order to further determine the desired solution area of the optimization problem, the boundaries for each variable are defined. These constraints are based on the physical boundaries of the electrical components. As an example, increasing the inductances results in increased weight and cost of the system. These constraints for the maximum and minimum values for the inductors, and resonant capacitors are defined as:

$$\begin{aligned} L_1^{min} \le L_1 \le L_1^{max} \\ C_1^{min} \le C_1 \le C_1^{max} \\ C_{s1}^{min} \le C_{s1} \le C_{s1}^{max} \\ C_{s2}^{min} \le C_{s2} \le C_{s2}^{max} \end{aligned} \quad (34)$$

In order to respond to the load demand, acceptable output voltage regulation is required for different loads at different coupling conditions (k). This behavior included in the optimization problem by defining a maximum and minimum voltage limit for the output voltage. In addition, it is preferred that the converter provides a constant output voltage for a wide range of output power (ΔP_{out}). The slope of the V_o-P_{out} plane is limited to the desired value ε_v. These voltage constraints are expressed in the following equations:

$$\frac{\partial V_o(P_{out},k)}{\partial P_{out}} \approx \frac{\Delta V_o(P_{out},k)}{\Delta P_{out}} \le \varepsilon_v \quad (35)$$

$$V_o^{min}(P_{out},k_i) \le V_o(P_{out},k) \le V_o^{max}(P_{out},k_i), \quad \forall k_i \in K_n \quad (36)$$

Furthermore, as it mentioned before, the LCC compensation network needs to provide a constant current in the primary coil independent of the load variations. This is addressed in the optimization problem as follows:

$$\frac{\partial I_p(P_{out},k)}{\partial P_{out}} \approx \frac{\Delta I_p(P_{out},k)}{\Delta P_{out}} \le \varepsilon_i \quad (37)$$

In practice, each circuit component has a maximum voltage or current ratings. Therefore, the valid operating range is included as described below:

$$I_p^{min}(P_{out},k) \le I_p(P_{out},k) \le I_p^{max}(P_{out},k) \quad (38)$$

$$I_s^{min}(P_{out},k) \le I_s(P_{out},k) \le I_s^{max}(P_{out},k) \quad (39)$$

In order to minimize no-load losses, a new constraint is defined in (13). In this case, assuming a very low value for k (long separation between couplers) an approximate no-load situation is observed from the primary side. In no-load condition, the inverter output current $I_{in}(P_{out},k)$, needs to be lower than a specific value:

$$I_{in}(P_{out},k_0) \le \varepsilon_{i0} \quad (40)$$

In (39), k_0 is a small value of k, which represents the absence of the secondary side condition. In this paper, k_0 is considered 2% of the maximum coupling coefficient. Selection of the ε_v, ε_i and k_0 is dependent on the designer experience and application desired values. In addition, if these values selected very small, the optimization may be diverged.

As it has been discussed before, the LCC compensated network should be designed to represent an inductive-resistive load for the inverter to achieve ZVS condition. The phase angle

of the input impedance should be limited as follows:

$$\phi^{\min} \le \phi(P_{out}, k) \le \phi^{\max} \quad (41)$$

Due to the parameter variations in experimental implementation, in practice the value of the $\phi^{\min}$ should be selected a positive value to satisfy ZVS condition in different operating points.

D. Optimal Solution

The proposed formulation has been applied to solve an optimization problem. This optimization has a high order of freedom for different variables, and there are too many possible solutions for this study. The problem needs to be solved in automatic optimization software. In this work, the Non-Linear Programming (NLP) optimization is performed in the General Algebraic Modeling System (GAMS) software using the Branch-And-Reduce Optimization Navigator (BARON) [43], [44]. BARON is a branch and bound type global tool to solve nonconvex NLP and Mixed Integer Non-Linear Programming (MINLP) optimization problems. The software can guarantee the global optimally of the solution under fair defined constraints, and boundaries. In this optimization method, the definition of the upper and lower bounds for each variable helps the solver to reduce the search area and find the optimal solution. In addition, the discussed solver benefits from a heuristic local search method which randomly initializes the solver to determine the bounds of unlimited variables. The validity of the solution is not based on the initial settings of the variables [45]. The optimization program will terminate the process when the problem is converging and reaches to a predefined acceptable absolute gap. Outputs of this optimization problem are the optimal values of resonant network elements: L_1, C_1, C_{s1}, and C_{s2}.

TABLE II
VARIABLES RANGES

Variable/Parameter	Min.	Max./Fix Value
L_1	1 µH	200 µH
C_1, C_{s1}, C_{s2}	1 nF	1000 nF
$V_o(P_{out}, k_2)$	150 V	200 V
$V_o(P_{out}, k_3)$	200 V	250 V
$V_o(P_{out}, k_4)$	250 V	300 V
$I_p(P_{out}, k)$	0	15 A
$I_s(P_{out}, k)$	0	15 A
ϕ	0.06	π/2
ε_v	-	8 V/kW
ε_i	-	10^{-4} A/W
ε_{i0}	-	0.5 A
V_{dc}	-	200 V
f	-	85 kHz

TABLE III
COMPONENT SPECIFICATIONS

Parameter	Value
$R_{ds(on)}$	45 $m\Omega$(@25°C)
r_1	50 $m\Omega$(@85 kHz)
r_p	382 $m\Omega$(@85 kHz)
r_s	394 $m\Omega$(@85 kHz)
tanδ(f)	10^{-3}(@100 kHz)

TABLE IV
DESIGN SPECIFICATIONS

Variable	Optimal Value	Conventional
L_1	73.4 µH	69.5 µH
C_1	46.7 nF	55.4 nF
C_{s1}	15.5 nF	14.6 nF
C_{s2}	11.7 nF	11.6 nF
$TWAE(k_2 = 0.2)$	92.3 %	90.9 %
$TWAE(k_3 = 0.3)$	94.6 %	93.0 %
$TWAE(k_4 = 0.35)$	95.1 %	93.4 %
Objective Value	2.78	-

These optimal values satisfy the design constraints and lead to have an efficient design over a wide range of loads and different coupling conditions. As a case study, the former optimization is performed for a 1 kW design. Based on the discussed weighted average efficiency method the nominal output power set is defined as P_n={700,800,900,180} and the weighted factors is considered as W_{pn}={0.033,0.767,0.126,0.074}. In this paper, the set of the nominal coupling coefficients is defined as K_n={0.2,0.3,0.35}. Table II, and III list the practical constraints and the values of the component specifications, respectively. Table IV presents the result of the constrained NLP problem. Fig. 7 illustrates the simulation results of the phase angle of the input impedance Z_{in}, as a function of output load. This can be inferred from (9-15) that in each coupling condition, the resistive load should be in a specific range to achieve ZVS. However, in this case for coupling of 0.2 to 0.35, the input phase angle on the primary side has a positive value which results in achieving ZVS condition for the whole output power ranges.

E. Comparison

A conventional design procedure of the primary side LCC compensation network based on other publications and its calculated TWAE values is listed in Table IV [14], [17]. Simulation results of the efficiency of the proposed optimized method and conventional method are compared in Fig. 8. It can be seen that the proposed LCC converter presented a higher efficiency all over the operating range. Especially, in light-load

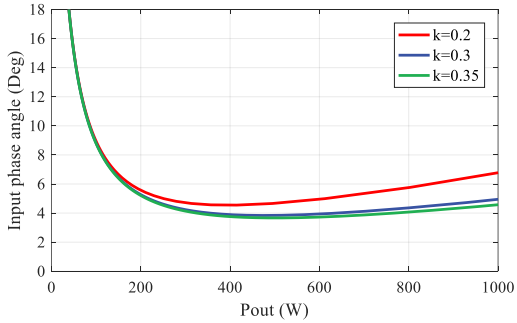

Fig. 7. Input phase angle of the optimized LCC converter versus output power in different coupling conditions

This article has been accepted for publication in a future issue of this journal, but has not been fully edited. Content may change prior to final publication. Citation information: DOI 10.1109/TIE.2018.2840502, IEEE Transactions on Industrial Electronics

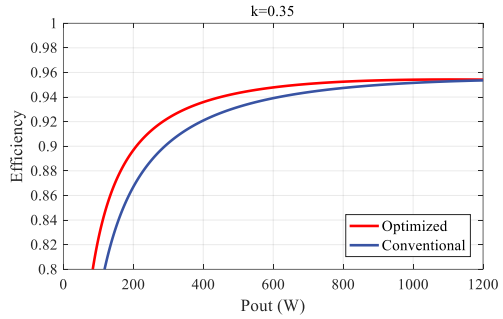

Fig. 8. Efficiency comparison between conventional and proposed

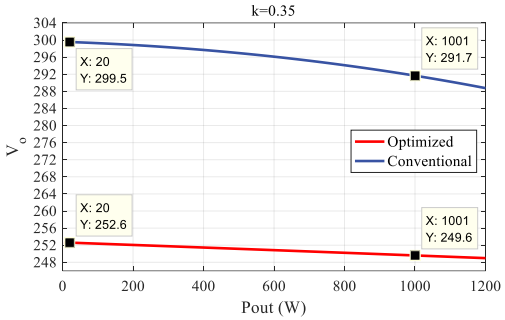

Fig. 9. Output voltage drop comparison between conventional and proposed method

condition, the proposed LCC converter has a better performance. The output voltage characteristics of the proposed method is illustrated in Fig. 9. The performance of the WPT system, in terms of the output voltage characteristics, is compared by calculating the slope of the V_o with respect to the output power. Although the voltage gain of the conventional circuit is higher, the output voltage has higher slope against output power too. The proposed method results in voltage to power slope of 3 V/kW versus 8 V/kW in case of the earlier method. Therefore, the proposed method offers better output voltage performance in comparison with the conventional design procedure. Hereby, the constraints defined in the optimization problem have properly addressed the design objectives.

IV. Experimental Results

To validate the proposed circuit, and the optimization results, a prototype of the optimized stationary WPT charging system with the circular magnetic pads has been implemented. The specification and measured values for the magnetic couplers

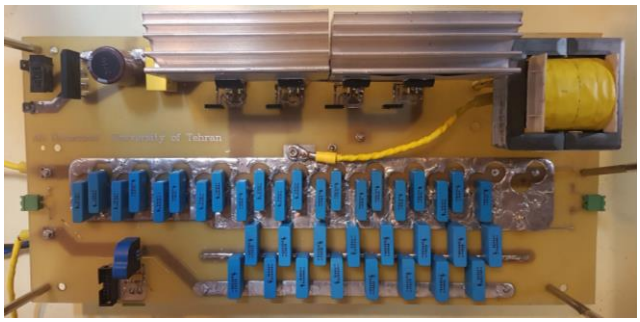

Fig. 10. Prototype of the LCC resonant converter for primary side

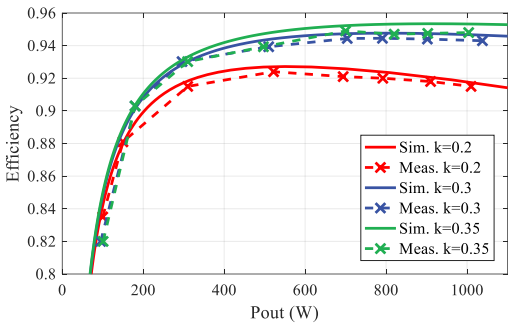

Fig. 11. System efficiency under different load and coupling conditions

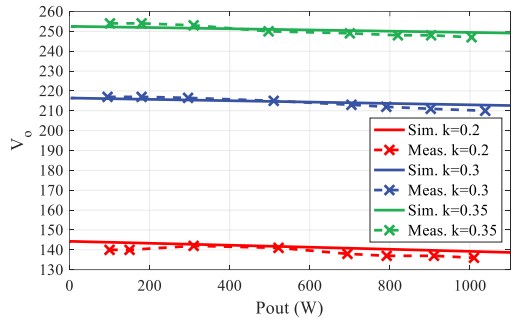

Fig. 12. Output voltage under different load and coupling conditions

were presented in section II. Fig. 10 shows the experimental setup. The resonant film capacitors are metalized film polypropylene (MFP) capacitors. These MFP capacitors are designed for high-frequency ac loads. The ferrite material type in all magnetic components is PL-7 from Samwha. STM 32 F407 ARM Cortex-M4, is used to implement the phase-shifted control and generate the gating signals for the primary side inverter. In this study, the open-loop measurements presented to focus on the design of the LCC-series compensated network and its output profiles. In this prototype, the inverter was built with a dc-link voltage of 200 V switches were 650 V MOSFET from Infineon. The inverter operating frequency is selected 85 kHz and the dc-to-dc efficiency measurements are presented in this section.

The measured system efficiency and output voltage curves are compared with the simulation results in Fig. 11 and Fig. 12. It can be seen that the efficiency curve is almost flat for the power range of 300 to 1000 W. Fig. 11 shows the output voltage is almost constant for a wide range of output power. Moreover, the experimental results are very close to the simulation results of the WPT converter. In Fig. 13 the waveforms of inverter output voltage and currents and the dc output voltage for 1 kW and 500 W loads are presented with an open-loop control circuit. Therefore, the phase shift of the inverter is manually set to 180 degrees and only the open-loop output voltage of the load side is measured. As can be seen, the inverter output current have a lag phase angle respect to the inverter output voltage. ZVS is achieved for all the loads below 1 kW and different coil positions. In this experimental study, the maximum efficiency was 94.8% in 1kW output with coupling condition of k=0.35.

V. Conclusion

This paper presented an optimal design method for an LCC-

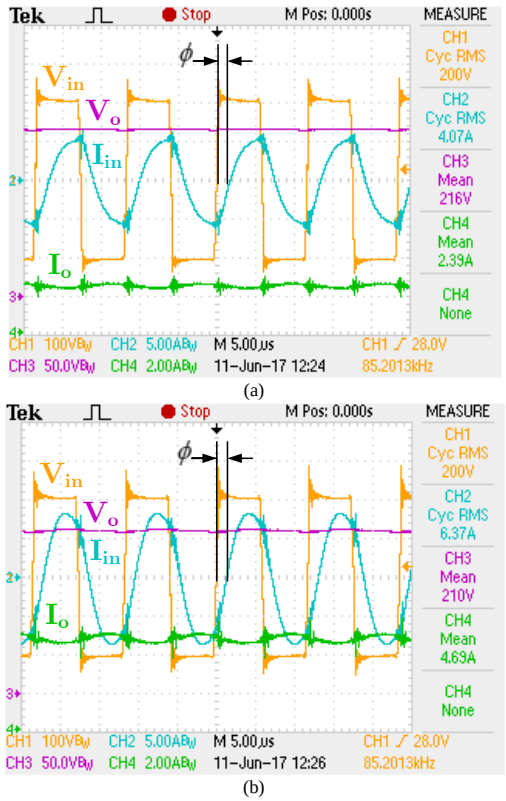

Fig. 13. Inverter and output waveforms for k=0.3 under (a) P_{out} =516.2 W and (b) P_{out} =984.9 W

series compensated resonant converter operating as a stationary WPT EV charger. The proposed topology was analyzed and modeled accurately to calculate the converter losses. The magnetic coupler losses are calculated to consider in optimal designing of the resonant converter. In stationary charging of EV, it is preferred to have a flat efficiency and output voltage curves for a wide range of output power and different coupling conditions. To achieve an optimal design, an optimization problem was defined in which the objective function included a time-weighted efficiency for all normal coupling conditions. Moreover, practical constraints such as current and voltage limits were applied. In order to guarantee the ZVS operating for the WPT system, the input phase angle of the primary side was defined as a positive value in the constraints of the optimization problem. The simulation results for the proposed converter showed that the input phase angle remained positive in different coupling and load conditions. The proposed optimized circuit was compared with a conventional design method. Although they both have high-efficiency profiles, the optimized converter presented a higher efficiency curve that was flatter. In addition, the proposed method resulted in a WPT system in which the output voltage is almost independent of the output variations. Moreover, the proposed method is flexible enough to be applied to different power ratings accommodating alternative practical limitations. A 1 kW hardware prototype was built to validate the proposed compensation network design. The results of the overall efficiency and output voltage in different loading and coupling conditions were presented. Owing to achieved ZVS condition, a peak efficiency of 94.8% at the coupling coefficient of 0.35 (an air gap of 125 mm) was measured.

VI. REFERENCES

[1] C. C. Mi, G. Buja, S. Y. Choi, and C. T. Rim, "Modern Advances in Wireless Power Transfer Systems for Roadway Powered Electric Vehicles," *IEEE Trans. Ind. Electron.*, vol. 63, no. 10, pp. 6533–6545, 2016.

[2] F. Lu, H. Zhang, H. Hofmann, and C. C. Mi, "A Dynamic Charging System with Reduced Output Power Pulsation for Electric Vehicles," *IEEE Trans. Ind. Electron.*, vol. 63, no. 10, pp. 6580–6590, 2016.

[3] S. Zhou and C. Chris Mi, "Multi-Paralleled LCC Reactive Power Compensation Networks and Their Tuning Method for Electric Vehicle Dynamic Wireless Charging," *IEEE Trans. Ind. Electron.*, vol. 63, no. 10, pp. 6546–6556, 2016.

[4] J. Shin, S. Shin, Y. Kim, S. Ahn, and S. Lee, "Design and Implementation of Shaped Magnetic Resonance Based Wireless Power Transfer System for Roadway-Powered Moving Electric Vehicles," no. c, pp. 1–14, 2013.

[5] R. Bosshard, U. Iruretagoyena, and J. W. Kolar, "Comprehensive Evaluation of Rectangular and Double-D Coil Geometry for 50 kW/85 kHz IPT System," *IEEE J. Emerg. Sel. Top. Power Electron.*, vol. 4, no. 4, pp. 1406–1415, 2016.

[6] R. Bosshard and J. W. Kolar, "Multi-Objective Optimization of 50 kW/85 kHz IPT System for Public Transport," *IEEE J. Emerg. Sel. Top. Power Electron.*, vol. 4, no. 4, pp. 1370–1382, 2016.

[7] C. Park, S. Lee, S. Y. Jeong, G. H. Cho, and C. T. Rim, "Uniform Power I-Type Inductive Power Transfer System With DQ-Power Supply Rails for On-Line Electric Vehicles," *IEEE Trans. Power Electron.*, vol. 30, no. 11, pp. 6446–6455, 2015.

[8] L. Zhao, S. Member, D. J. Thrimawithana, U. K. Madawala, and S. Member, "IEEE TRANSACTIONS ON INDUSTRIAL ELECTRONICS A Hybrid Bi-directional Wireless EV Charging System Tolerant to Pad Misalignment," vol. 46, no. c, 2017.

[9] S. Li and C. C. Mi, "Wireless power transfer for electric vehicle applications," *IEEE J. Emerg. Sel. Top. Power Electron.*, vol. 3, no. 1, pp. 4–17, 2015.

[10] M. Budhia, J. T. Boys, G. Covic, and C.-Y. Huang, "Development of a single-sided flux magnetic coupler for electric vehicle IPT charging systems," *Ind. Electron. IEEE Trans.*, vol. 60, no. 1, pp. 318–328, 2013.

[11] R. Bosshard and J. W. Kolar, "All-SiC 9.5 kW/dm3 On-Board Power Electronics for 50 kW/85 kHz Automotive IPT System," *IEEE J. Emerg. Sel. Top. Power Electron.*, vol. 5, no. 1, pp. 419–431, 2017.

[12] R. Bosshard, J. W. Kolar, J. M??hlethaler, I. Stevanovi??, B. Wunsch, and F. Canales, "Modeling and η-α-pareto optimization of inductive power transfer coils for electric vehicles," *IEEE J. Emerg. Sel. Top. Power Electron.*, vol. 3, no. 1, pp. 50–64, 2015.

[13] A. Tejeda, C. Carretero, J. T. Boys, and G. A. Covic, "Core-less Circular Pad with Controlled Flux Cancellation for EV Wireless Charging," *IEEE Trans. Power Electron.*, vol. PP, no. 99, p. 1, 2016.

[14] B. Esteban, M. Sid-Ahmed, and N. C. Kar, "A Comparative Study of Power Supply Architectures in Wireless EV Charging Systems," *IEEE Trans. Power Electron.*, vol. 30, no. 11, pp. 6408–6422, 2015.

[15] T. Diekhans and R. W. De Doncker, "A Dual-Side Controlled Inductive Power Transfer System Optimized for Large Coupling Factor Variations and Partial Load," *Power Electron. IEEE Trans.*, vol. 30, no. 11, pp. 6320–6328, 2015.

[16] Z. Cong *et al.*, "High-Efficiency Contactless Power Transfer System for Electric Vehicle Battery Charging Application," *Emerg. Sel. Top. Power Electron. IEEE J.*, vol. 3, no. 1, pp. 65–74, 2015.

[17] H. H. Wu, A. Gilchrist, K. D. Sealy, and D. Bronson, "A high efficiency 5 kW inductive charger for EVs using dual side control," *Ind. Informatics, IEEE Trans.*, vol. 8, no. 3, pp. 585–595, 2012.

[18] A. Kamineni, G. A. Covic, and J. T. Boys, "Analysis of Coplanar Intermediate Coil Structures in Inductive Power Transfer Systems," *Power Electron. IEEE Trans.*, vol. 30, no. 11, pp. 6141–6154, 2015.

[19] Z. Cong, M. Hongbo, L. Jih-sheng, and Z. Lanhua, "Design Considerations to Reduce Gap Variation and Misalignment Effects for the Inductive Power Transfer System," *Power Electron. IEEE Trans.*, vol. 30, no. 11, pp. 6108–6119, 2015.

[20] J. P. K. Sampath, A. Alphones, S. Member, and D. Mahinda,

"Optimization of Wireless Power Transfer System with a Repeater Against Load Variations," vol. 46, no. c, 2017.

[21] X. Liu and G. Wang, "A Novel Wireless Power Transfer System With Double Intermediate Resonant Coils," *IEEE Trans. Ind. Electron.*, vol. 63, no. 4, pp. 2174–2180, 2016.

[22] D. Ahn and S. Hong, "A Study on Magnetic Field Repeater in Wireless Power Transfer," *IEEE Trans. Ind. Electron.*, vol. 60, no. 1, pp. 360–371, 2013.

[23] B. Esteban, N. Stojakovic, M. Sid-Ahmed, and N. C. Kar, "Development of mutual inductance formula for misaligned planar circular spiral coils," in *2015 IEEE Energy Conversion Congress and Exposition (ECCE)*, 2015, pp. 1306–1313.

[24] W. Zhang and C. C. Mi, "Compensation Topologies of High-Power Wireless Power Transfer Systems," *IEEE Trans. Veh. Technol.*, vol. 65, no. 6, pp. 4768–4778, 2016.

[25] W. Li, H. Zhao, J. Deng, S. Li, and C. C. Mi, "Comparison Study on SS and double-sided LCC compensation topologies for EV/PHEV Wireless Chargers," *IEEE Trans. Veh. Technol.*, vol. 65, no. 6, pp. 4429–4439, 2016.

[26] J. L. Villa, J. Sallan, J. F. Sanz Osorio, and A. Llombart, "High-Misalignment Tolerant Compensation Topology For ICPT Systems," *Ind. Electron. IEEE Trans.*, vol. 59, no. 2, pp. 945–951, 2012.

[27] M. K. Kazimierczuk and D. Czarkowski, *Resonant power converters*. John Wiley & Sons, 2012.

[28] T. Kan, T. D. Nguyen, J. C. White, R. K. Malhan, and C. C. Mi, "A new integration method for an electric vehicle wireless charging system using LCC compensation topology: Analysis and design," *IEEE Trans. Power Electron.*, vol. 32, no. 2, pp. 1638–1650, 2017.

[29] H. Chang-Yu, J. E. James, and G. A. Covic, "Design Considerations for Variable Coupling Lumped Coil Systems," *Power Electron. IEEE Trans.*, vol. 30, no. 2, pp. 680–689, 2015.

[30] S. Weearsinghe, D. J. Thrimawithana, and U. K. Madawala, "Modeling bidirectional contactless grid interfaces with a soft DC-link," *IEEE Trans. Power Electron.*, vol. 30, no. 7, pp. 3528–3541, 2015.

[31] M. J. Neath, A. K. Swain, U. K. Madawala, and D. J. Thrimawithana, "An Optimal PID Controller for a Bidirectional Inductive Power Transfer System Using Multiobjective Genetic Algorithm," *Power Electron. IEEE Trans.*, vol. 29, no. 3, pp. 1523–1531, 2014.

[32] M. Borage, S. Tiwari, and S. Kotaiah, "Analysis and design of an LCL-T resonant converter as a constant-current power supply," *IEEE Trans. Ind. Electron.*, vol. 52, no. 6, pp. 1547–1554, 2005.

[33] W. Li, S. Member, C. C. Mi, and S. Li, "Integrated LCC Compensation Topology for Wireless Charger in Electric and Plug-in Electric Vehicles," vol. 46, no. c, 2014.

[34] H. Feng, T. Cai, S. Duan, J. Zhao, X. Zhang, and C. Chen, "An LCC-Compensated Resonant Converter Optimized for Robust Reaction to Large Coupling Variation in Dynamic Wireless Power Transfer," *IEEE Trans. Ind. Electron.*, vol. 63, no. 10, pp. 6591–6601, 2016.

[35] Z. Fang, T. Cai, S. Duan, and C. Chen, "Optimal design methodology for llc resonant converter in battery charging applications based on time-weighted average efficiency," *IEEE Trans. Power Electron.*, vol. 30, no. 10, pp. 5469–5483, 2015.

[36] R. L. Steigerwald, "A comparison of half-bridge resonant converter topologies," *Power Electron. IEEE Trans.*, vol. 3, no. 2, pp. 174–182, 1988.

[37] X. Huafeng, G. Liang, and X. Shaojun, "A new ZVS bidirectional DC-DC converter with phase-shift plus PWM control scheme," *Conf. Proc. - IEEE Appl. Power Electron. Conf. Expo. - APEC*, vol. 23, no. 2, pp. 943–948, 2007.

[38] H. Wu, Y. Lu, K. Sun, and Y. Xing, "Phase-Shift-Controlled Isolated Buck-Boost Converter With Active-Clamped Three-Level Rectifier (AC-TLR) Featuring Soft-Switching Within Wide Operation Range," *IEEE Trans. Power Electron.*, vol. 31, no. 3, pp. 2372–2386, 2016.

[39] F. Liu, W. Lei, T. Wang, C. Nie, and Y. Wang, "A phase-shift soft-switching control strategy for dual active wireless power transfer system," in *2017 IEEE Energy Conversion Congress and Exposition (ECCE)*, 2017, pp. 2573–2578.

[40] M. Budhia, G. A. Covic, and J. T. Boys, "Design and Optimization of Circular Magnetic Structures for Lumped Inductive Power Transfer Systems," *Power Electron. IEEE Trans.*, vol. 26, no. 11, pp. 3096–3108, 2011.

[41] R. P. Wojda and M. K. Kazimierczuk, "Winding resistance of litz-wire and multi-strand inductors," *IET Power Electron.*, vol. 5, no. 2, p. 257, 2012.

[42] S. Wang and D. Dorrell, "Copper Loss Analysis of EV Charging Coupler," *Magn. IEEE Trans.*, vol. PP, no. 99, p. 1, 2015.

[43] M. Tawarmalani and N. V Sahinidis, "A polyhedral branch-and-cut approach to global optimization," *Math. Program.*, vol. 103, no. 2, pp. 225–249, 2005.

[44] N. V Sahinidis, "BARON: A general purpose global optimization software package," *J. Glob. Optim.*, vol. 8, no. 2, pp. 201–205, 1996.

[45] N. S. M. Tawarmalani, "BARON 17.1.2: Global Optimization of Mixed-Integer Nonlinear Programs." User's Manual, 2017.

Ali Ramezani (S'18) received the B.Sc. degree in electrical engineering from Shahid Beheshti University, Tehran, Iran, in 2014 and M.Sc. degree in electrical engineering from University of Tehran, Tehran, Iran, in 2017. He is currently a PhD student at Department of Electrical and Computer Engineering, McMaster University, Hamilton, Canada.

His research interests include design and control converters for electric vehicle applications, wireless power transfer and renewable energy sources.

Shahrokh Farhangi (M'90) obtained the B.Sc., M.Sc. and Ph.D. degrees in electrical engineering from University of Tehran, Iran, with honors. He is currently professor of School of Electrical and Computer Engineering, University of Tehran.

His research interests include design and modeling of Power Electronic Converters, Drives, Photovoltaics and Renewable Energy Systems. He has published more than 100 papers in conference proceedings and journals. He has managed several research and industrial projects, which some of them have won national and international awards. He has been selected as the distinguished engineer in electrical engineering by Iran Academy of Sciences, in 2008.

Hossein Iman-Eini (M'10-SM'17)received the B.S. and M.S. degrees from the University of Tehran, Iran in 2001 and2003, respectively, and the Ph.D. degree jointly from the University of Tehran and the Grenoble INP, Grenoble, France in2009, all in electrical engineering. He is currently an Associate Professor in the School of ECE, University of Tehran.

His current research interests include the modeling and control of power converters and renewable energy systems.

Babak Farhangi (S'99–M'08–SM'15) received the B.S. and M.S. degrees with honors from the University of Tehran, Tehran, Iran, in 2003 and 2006, respectively, and the Ph.D. degree from Texas A&M University, College Station, TX, USA, in 2014, all in Electrical Engineering.

He is currently a principal scientist at the research and development department, GAF, Parsippany, NJ, USA. Prior to GAF, Dr. Farhangi has been involved in product and technology development through several appointments in industry and academia. His research interests include power electronics and its applications in renewable energy systems, photovoltaics, energy storage, electric vehicles, and integrated power systems.

Ramin Rahimi received the B.Sc. degree in electrical engineering with honors from the University of Tabriz, Tabriz, Iran, in 2013, and M.Sc. degree in electrical engineering with honors from the University of Tehran, Tehran, Iran, in 2016. He is currently a researcher and laboratory instructor in the Department of Electrical and Computer Engineering, University of Tehran, Tehran, Iran.

His research interests include design, modeling, and digital control implementation of power electronics converters, renewable energy systems, grid-connected photovoltaic systems, wireless power transfer, and motor drives.

Gholam Reza Moradi received the B.Sc. degree in electrical engineering from Tafresh University, Tafresh, Iran, in 2013 and M.Sc. degree in electrical engineering from University of Tehran, Tehran, Iran, in 2016. He is currently a researcher at Department of Electrical and Computer Engineering, University of Tehran, Tehran, Iran.

His research interests include design and control of power converters for renewable energy systems, control strategies for grid integration of renewable energy sources, and digital control implementation.